euronoise

Identification of noise sources by means of inverse finite element method using measured data

Matthias Weber, Thomas Kletschkowski and Delf Sachau

Helmut-Schmidt-Universität - Universität der Bundeswehr Hamburg, Holstenhofweg 85, 22043 Hamburg, Germany
mweber@hsuhh.de

Identification of noise sources in aircraft cabins proves to be difficult particularly at low frequencies. A new approach, based on the Inverse Finite Element Method, reconstructs the spatial distribution of sound pressure and particle velocity.

This procedure requires measurements in the cavity first. If all sound sources are located on the boundary, the equation system resulting from a matching FE model can be re-sorted in such a way that computation of the unknown boundary data is possible, even with distorted measurement data.

The method is validated using a simplified 2D laboratory experiment consisting of a flat rectangle with sound-hard boundary in which a loudspeaker is included. A corresponding numerical model is verified by mapping the sound pressure in the test bed. The inner part of the measurement data is used to compute the boundary data.

To prepare a validation of this technique in real world conditions, the sound field in the cavity of an aircraft mock-up (Airbus A340) excited by both interior and exterior noise sources is mapped with a custom-built microphone array. A matching FE model is verified and compared to the measured data.

1 Introduction

Aircraft cabin noise causes a severe limitation of the passengers' comfort. To localize acoustic hot spots, i.e. the main sources in the structure where sound is transmitted into the cabin, several techniques have been established, ranging from simple sound pressure or intensity measurements to more advanced methods such as Beamforming [1, 2], Acoustic Holography [3, 4, 5, 6], or Inverse Boundary Element Method (IBEM) [7]. Most of these techniques, however, are either highly ineffective or demand creating artificial free-field conditions to avoid standing waves.

Therefore, a novel approach has been introduced to identify acoustic hot spots using an inverse finite element method (IFEM), see [8, 9, 10]. This technique is insensitive to standing waves and for this reason highly qualified for interior noise problems.

The approach presented in this paper will be applied to reconstruct the distribution of sound pressure and particle velocity in the interior of the cabin based on a standard FE model. From a certain subspace of the interior, referred to as measurement area, data are taken and used as boundary conditions for the IFEM that will predict the sound field in the complete area, including the boundaries between interior and structure. Examining sound pressure and particle velocity on these boundaries, conclusions can be drawn to the location of acoustic hot spots.

2 Noise Source Identification by inverse FEM

The FE method for the time-harmonic analysis of weakly damped interior noise problems is based on the Helmholtz equation

$$\Delta p(\mathbf{x}) + k^2 p(\mathbf{x}) = 0\,, \tag{1}$$

where Δ represents the Laplace operator and $k = 2\pi f / c$ the wave number that is determined by the excitation frequency f and the speed of sound c. The corresponding boundary conditions (BC) are given by the Dirichlet BC for the acoustic pressure

$$p = \overline{p} \quad \text{on } R_p\,, \tag{2}$$

and the Neumann BC for the normal component of particle velocity

$$-\mathbf{n}\cdot\frac{1}{\rho}\nabla p = i(2\pi f)\overline{v}_n \quad \text{on } R_v\,. \tag{3}$$

Discretization of Eq. (1) using the FE method leads to a set of algebraic equations for the sound pressure that can be summarized as

$$\mathbf{K}\mathbf{p} = \mathbf{v}\,. \tag{4}$$

$\mathbf{K}$ is the stiffness matrix, $\mathbf{p}$ the vector of the excess pressure and $\mathbf{v}$ a vector that is proportional to the particle velocity in the sound field, and therefore called generalized velocity vector. The solution of Eq. (4) with respect to the BC leads to the unknown pressure field $\mathbf{p}$. This process is called forward calculation.

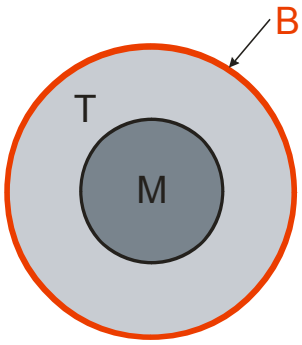

Fig. 1: Spatial domain decomposition

In order to derive the IFEM the calculation domain is split into three regions: an inner measurement sub-domain (M), a transition sub-domain (T), and an outer boundary (B) as illustrated in Fig. 1. It is possible to decompose Eq. (4) as follows:

$$\begin{bmatrix} \mathbf{K}_1 & \mathbf{K}_2 & \mathbf{K}_3 \\ \mathbf{K}_4 & \mathbf{K}_5 & \mathbf{K}_6 \\ \mathbf{K}_7 & \mathbf{K}_8 & \mathbf{K}_9 \end{bmatrix} \begin{bmatrix} \mathbf{p}_{MK} \\ \mathbf{p}_{TU} \\ \mathbf{p}_{BU} \end{bmatrix} = \begin{bmatrix} \mathbf{v}_{MK} \\ \mathbf{v}_{TK} \\ \mathbf{v}_{BU} \end{bmatrix}. \tag{5}$$

The first index of the three sound pressure sub-matrices $\mathbf{p}_{ij}$ and the three sub-matrices $\mathbf{v}_{ij}$ of the generalized velocity vector $\mathbf{v}$ denotes the sub-domain of the decomposed

calculation domain, whereas the second index denotes whether the variable is known (K) or unknown (U).

As described in [10], in the absence of unknown volume sources in the transition and measurement sub-domain the unknown parts of the sound pressure vector **p** can be computed by the solution of a reduced problem that is given by

$$\begin{bmatrix} \mathbf{K}_2 & \mathbf{K}_3 \\ \mathbf{K}_5 & \mathbf{K}_6 \end{bmatrix} \begin{bmatrix} \mathbf{p}_{TU} \\ \mathbf{p}_{BU} \end{bmatrix} = \begin{bmatrix} -\mathbf{K}_1 \mathbf{p}_{MK} \\ -\mathbf{K}_4 \mathbf{p}_{MK} \end{bmatrix}. \tag{6}$$

The solution of

$$\begin{bmatrix} \mathbf{K}_8 & \mathbf{K}_9 & -\mathbf{I} \end{bmatrix} \begin{bmatrix} \mathbf{p}_{TU} \\ \mathbf{p}_{BU} \\ \mathbf{v}_{BU} \end{bmatrix} = \begin{bmatrix} -\mathbf{K}_7 \mathbf{p}_{MK} \end{bmatrix} \tag{7}$$

leads to the unknown velocities at the outer boundary. This procedure is called inverse calculation.

Eq. (6) can be solved to determine the complete sound field in the interior using only the measurements in the inner region of the sound field. For simplicity it is rewritten as follows:

$$\mathbf{A}\mathbf{x} = \mathbf{b}\,; \tag{8}$$

$$\mathbf{A} \equiv \begin{bmatrix} \mathbf{K}_2 & \mathbf{K}_3 \\ \mathbf{K}_5 & \mathbf{K}_6 \end{bmatrix}, \mathbf{x} \equiv \begin{bmatrix} \mathbf{p}_{TU} \\ \mathbf{p}_{BU} \end{bmatrix}, \mathbf{b} \equiv \begin{bmatrix} -\mathbf{K}_1 \mathbf{p}_{MK} \\ -\mathbf{K}_4 \mathbf{p}_{MK} \end{bmatrix}.$$

As stated in [8] it has been found that the condition number of the new portioned stiffness matrix **A** is very high, especially if realistic measurement errors are taken into account. Therefore, several regularization techniques such as Truncated Singular Value Decomposition (TSVD), Tikhonov Regularization (TR) or Conjugated Gradient Least Squares (CGLS) have been applied to solve the ill-posed problem that is given by Eq. (8).

More details about the regularization algorithms that have been used to solve Eq. (8) can be found in previous publications. The implementation of the TSVD and TR is described in [8, 9, 10].

3 2D Validation in a Laboratory Experiment

The experimental validation of the IFEM was first realized in a simplified laboratory test bed. In this, standing waves could only propagate in two dimensions, so that the third dimension did not have to be taken into account. The cavity to be measured was enclosed hermetically in a cuboid formed by laminated fiberboard and acrylic glass. Length and width of the test bed were l = 0.70m and b = 0.50 m, the height was set h = 0.13m to prevent the propagation of modes below $f_{max} = c/2h$ = 1320Hz. This is sufficiently greater than the frequency range to be considered (f < 500Hz), so a two-dimensional FE model could be applied. The boundaries were estimated to be sound-hard, accordingly no damping was introduced in the FE model. A loudspeaker was included in the border to induce vibrations to the enclosed cavity. Its position was to be determined by the IFEM.

As the mesh nodes of the corresponding FE model should be used as measurement positions at the same time and therefore be distributed uniformly, a refinement of the mesh towards the edges of the calculation domain was abandoned. However, this could have negative effects on the quality of the model. In order to compensate for these, an attempt was made to weaken the influence of the edge singularities by adding four bevels to the edges (see Fig. 2).

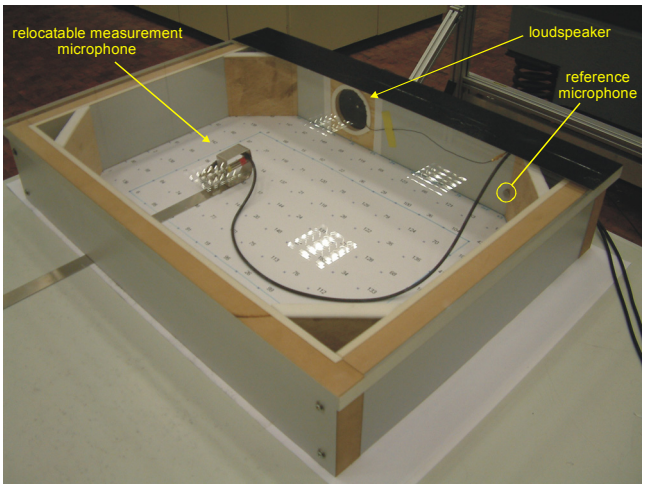

Fig. 2: Test bed with bevels, mesh nodes and relocatable measurement microphone

The mesh consisted of triangular elements with linear Lagrange trial functions and 165 respectively 153 degrees of freedom (DOF). The 2D model was validated by comparing the measured and numerically calculated resonance frequencies for f < 500Hz. The mesh nodes were transferred to the footpoint of the test bed.

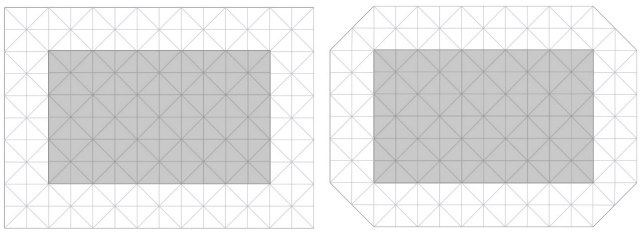

Fig. 3: FE mesh with 165 (left) resp. 153 DOF (with bevels, right) and highlighted inner measurement sub-domain

In the following, the inner measurement sub-domain was defined, the sound pressure at the included nodes being captured as initial data for the IFEM (77 nodes, see Fig. 3).

The system was excited with tonal noise at different frequencies. Power spectrum and phase in relation to a reference microphone were recorded for each position in the measurement sub-domain. In addition, as a benchmark for the inverse calculation, also the values on the outer boundary were measured.

In the FE model, the forward calculation was performed with a normal acceleration BC simulating the loudspeaker, its amplitude being determined by the acceleration measured on the loudspeaker membrane.

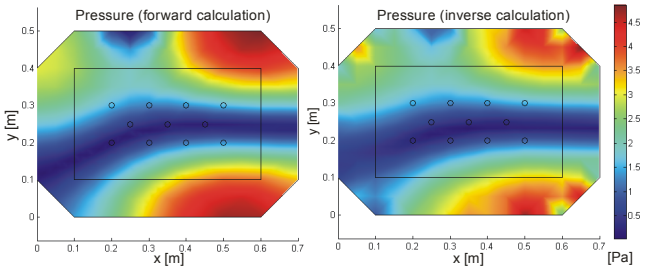

Fig. 4: Comparison of magnitude of sound pressure. Left: forward calculation; right: measured data (inner sub-domain) and inverse calculation (outer sub-domain)

Fig. 4 compares the numerically calculated distribution of the sound pressure to the measured and inversely calculated values of the sound field attuning for excitation with f = 400Hz. As a regularization technique, the TSVD was applied; the regularization parameter was chosen via L-curve method [11].

The position of the sound source (x = 0.25m; y = 0.5m) is clearly recognizable in both cases. However, the oscillations on the boundary that are typical for ill-posed problems could not be fully eliminated. Possible causes for this are the suboptimal mesh, the edge singularities and the standard algorithm to find the optimal regularization parameter; these are subject to further investigations.

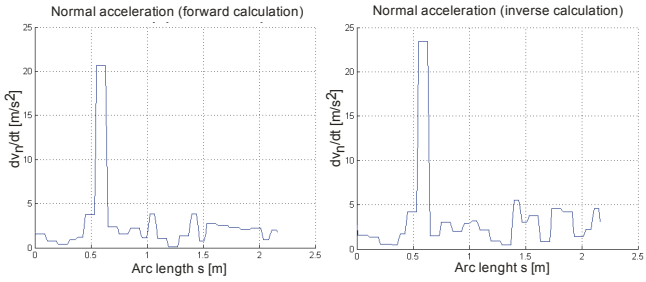

Fig. 5: Behaviour of the normal acceleration along the outer boundary. Left: forward calculation; right: inverse calculation

More significant for the identification of sound sources than the pressure, however, is the particle velocity, because its normal component must be zero at sound-hard boundaries. As a consequence, a particle velocity distinctly greater or less than zero indicates a sound source or sink at the corresponding position. The particle velocity is derived from the sound pressure according to Euler's equation

$$\rho \frac{dv}{dt} = -\nabla p \,, \qquad (9)$$

where ρ represents the density of air and ∇ the del operator. Fig. 5 shows the behavior of the normal acceleration dv/dt as a function of the arc length s along the outer boundary, in both forward and inverse calculation. Despite the oscillations of the sound pressure mentioned above, the position of the sound source can be identified clearly at s = 0.6m in both cases; also the magnitudes coincide well.

4 3D Validation in an Aircraft Mock-up

4.1 Mapping of the Mock-up

In the next validation step, the IFEM will be applied in a more realistic experiment realized in an Airbus A-340 fuselage segment. For that purpose, the three-dimensional sound field in the cabin of the mock-up was mapped with a custom built microphone array for two types of excitation:

1. wideband noise excitation by a loudspeaker inside the cabin,
2. wideband noise excitation by two loudspeakers outside of the cabin, located on each side of the fuselage where the engines would normally be.

The first case has the advantage that the position of the noise source is known and can be compared to the result of the inverse calculation, so this experiment serves for validation of the IFEM. The second case is another step towards real-world conditions. The fuselage segment is fully equipped with floor, lining and hat racks; the seats have been removed to achieve more controllable conditions. The ends are closed with absorbing foam wedges to approach free field conditions in the corresponding direction (z axis). Fig. 6 shows the mock-up and the built-in measuring apparatus.

Fig. 6: Aircraft mock-up (left), measuring apparatus (right)

The mapping was done using a uniform three-dimensional grid with a distance of d = 0.17m between the measuring positions, resulting in a total of 7172 positions. A line array of up to 31 microphones (x = 1..31) was therefore moved along y axis (14 positions, y = 1..14) and z axis (22 positions, z = 1..22). The dimensions of the mock-up and the grid are illustrated in Fig. 7.

Again, power spectrum and phase in relation to a reference were recorded. For a later validation of the IFEM, the lining

was roughly scanned with a sound intensity probe to find hot spots. In addition, accelerometers were fixed on some of these.

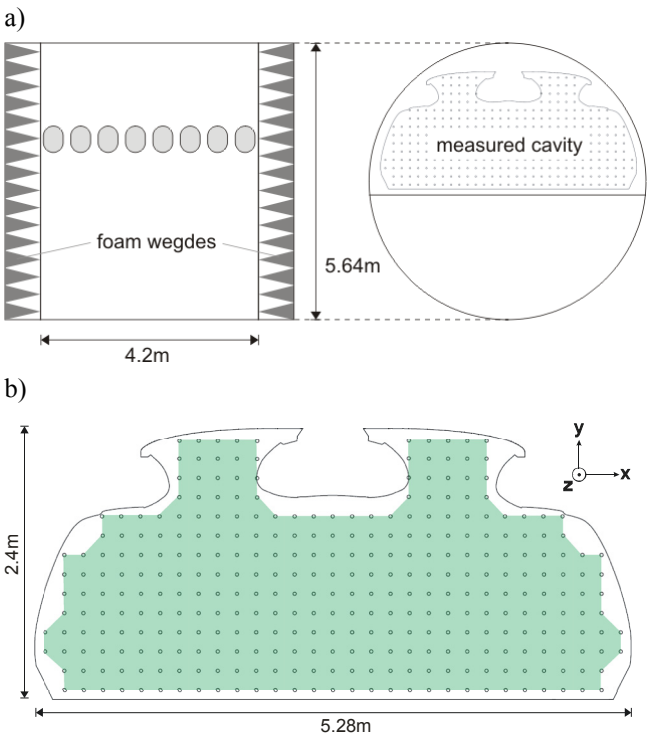

Fig. 7: Dimensions of the mock-up (a) and the measured cavity (b) including measuring grid

4.2 Validation of the FE Model

In order to verify the corresponding FE model of the cavity as shown in Fig. 8, its convergence had to be secured. For this purpose, all boundaries were defined to be sound-hard. Ten eigenfrequencies around 200Hz were numerically calculated for different meshes with a growing number of DOF. This was achieved by relating the maximum element size to the wavelength λ, correlating to a maximum frequency of $f_{\max}$ = 300Hz:

$$d_{\max} = \lambda / n; \quad \lambda = c / f_{\max}; \quad n = 4,5,...,11. \qquad (9)$$

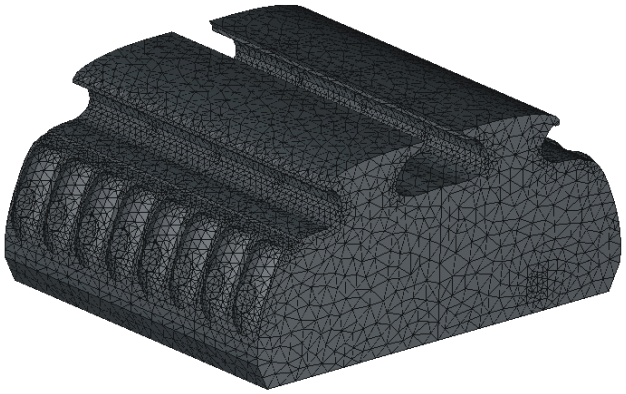

Fig. 8: FE model of the cavity

Since the distance between the single eigenfrequencies had the same order of magnitude as the amount each eigenfrequency decreased with every step of refinement, the matching eigenfrequencies were identified using the Modal Assurance Criterion (MAC)

$$\frac{\left|\{\psi_A\}^H \{\psi_B\}\right|^2}{\{\psi_A\}^H \{\psi_A\} \{\psi_B\}^H \{\psi_B\}}. \qquad (10)$$

The MAC is a scalar constant rating the causal relationship between two modal vectors $\{\psi_A\}$ and $\{\psi_B\}$. It takes on values between zero, implying no consistent correspondence, to one, signifying a consistent correspondence [12]. By means of the MAC, the variances of eight eigenfrequencies could be monitored with growing mesh refinement. In Fig. 9, the number of DOF is plotted against the variance of each eigenfrequency from one refinement step to another. For the step from 69266 DOF to 92084 DOF, the variance is less than 0.1 %, so 69266 DOF corresponding to $d_{\max} = \lambda/9$ is considered sufficient.

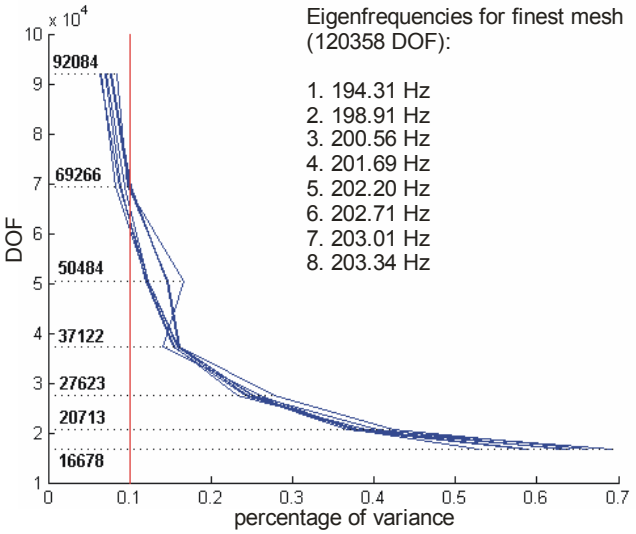

Fig. 9: Convergence of the FE model

4.3 Comparison of Model and Mapping

In the mock-up, the ends of the fuselage are not sound-hard but closed with absorbing material. However, for the application of the IFEM no *a priori* information on the boundary impedance is necessary – on the contrary, the boundary impedance can be deduced from the results of the IFEM (a near free field impedance resulting for the fuselage ends may be another factor for the validation of the IFEM). Nevertheless, to perform a forward calculation that roughly estimates the sound field excited by the internal loudspeaker, the ends were given a free field impedance BC. A normal acceleration BC was applied at the location of the loudspeaker, and the remaining boundaries were left sound-hard.

a) numerical result ($z = 11, f = 293$Hz)

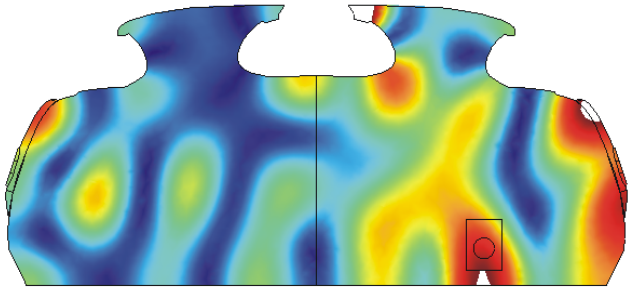

b) measured data ($z = 11, f = 293$Hz, internal loudspeaker)

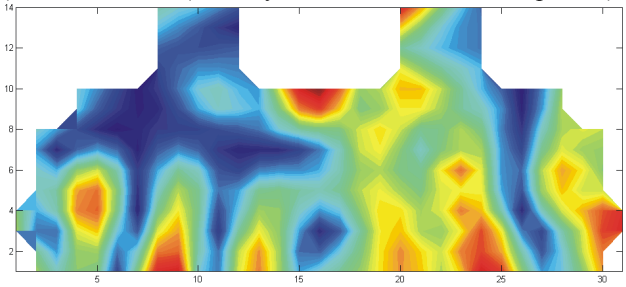

c) measured data ($z = 11, f = 293$Hz, external loudspeaker)

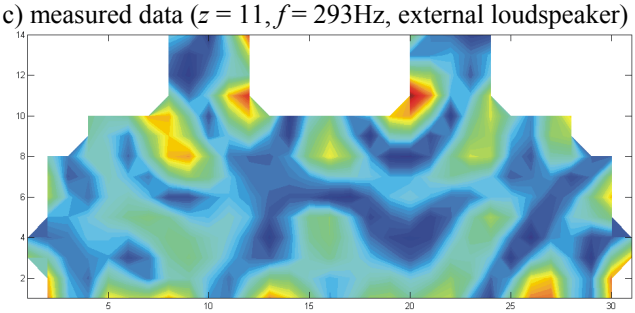

Fig. 10: Slice plots for numerical result (a) and measured data with internal (b) and external (c) loud-speaker. (a) contains the position of the speaker near $z = 22$. Shown is the magnitude of the sound pressure in linear scale.

Fig. 10 illustrates a slice plot of the symmetry plane of the fuselage referring to the two ends ($z = 11$), of the numerical result for $f = 293$Hz and the corresponding plots for internal and external loudspeaker excitation. This frequency was chosen because it showed a significant peak on a number of frequency response plots of the measured data. The amplitude values are not significant in these plots; the scale was adapted to enable merely a qualitative comparison. Despite the rough estimation of the BC, there are obvious similarities between the numerical result and the measured data for internal excitation. For excitation with the external speaker, however, the distribution of sound pressure differs significantly.

5 Summary and Outlook

In the first part of this paper, an inverse finite element method for noise source identification has been presented. In order to verify the IFEM, a laboratory experiment has been successfully applied using a simplified two-dimensional test bed. The original sound field as well as the location of the sound source could be reconstructed.

In the second part, the verification of the IFEM method in three-dimensional, more real-life conditions has been prepared. The cavity of an aircraft mock-up was mapped, a matching FE model was validated, and the sound pressure distribution of both has been compared.
In ongoing work, the IFEM algorithm will be extended to three dimensions and an inverse calculation shall be performed using part of the mapped data.

Acknowledgments

The authors would like to thank Mr. Kai Simanowski and Mr. Oliver Pabst (Professorship for Mechatronics) as well as Mr. Bernhard Samtleben (Airbus) for their support during the mapping of the mock-up, and Airbus for financial support.

References

[1] J. Christensen, J. Hald, “Beamforming”, Technical Review, Brüel & Kjaer, No. 1 (2004)

[2] K. R. Holland, P. A. Nelson, “Sound source characterisation: The focused beamformer vs the inverse method”, 10th Int. Congress on Sound and Vibration, Stockholm (2003)

[3] J. Hald, “Non-stationary STSF”, Technical Review, Brüel & Kjaer, No. 1 (2000)

[4] J. D. Maynard, E.G. Williams, Y. Lee, “Nearfield acoustic holography: Theory of generalized holography and the development of NAH”, *J. Acoust. Soc. Am.* 78(4), 1395-1413 (1985)

[5] R. Reibold, “Sound source reconstruction using fourier optics”, *Acustica* 63, 60-64 (1987)

[6] E. G. Williams, “Fourier Acoustics”, Academic Press, London (1999)

[7] N. Vlahopoulos, S. T. Raveendra, “Formulation, implementation and validation of multiple connection and free edge constraints in an indirect boundary element formulation”, *J. Sound Vib.* 210(1), 137-152 (1998)

[8] J. Drenckhan, D. Sachau, “Identification of sound sources using inverse FEM”, Proceedings of the 11th Int. Congress on Sound and Vibration, Stockholm (2003)

[9] J. Drenckhan, D. Sachau, “Identification of sound sources using inverse FEM”, 7th Int. Symposium “Transport Noise and Vibration“, St. Petersburg (2004)

[10] D. Sachau, J. Drenckhan, T. Kletschkowski, S. Petersen, “Entwicklung von Messtechniken zur Lärmquellenidentifizierung in Kabinen“, Final report LUFO HH TUT-34, Helmut Schmidt University/ University of the Federal Armed Forces Hamburg (2005)

[11] P. C. Hansen, “Rank-Deficient and Discrete Ill-Posed Problems”, Vol. 1, Society for Industrial and Applied Mathematics, Philadelphia (1998)

[12] R. J. Allemang, D. L. Brown, "A Correlation Coefficient for Modal Vector Analysis", Proceedings, Int. Modal Analysis Conference, 110-116 (1982)